ISSN 2075-1087, Gyroscopy and Navigation, 2021, Vol. 12, No. 2, pp. 178–185. © Pleiades Publishing, Ltd., 2021.
Russian Text © The Author(s), 2021, published in Giroskopiya i Navigatsiya, 2021, Vol. 29, No. 2, pp. 97–109.

A Study on the Effect Produced by Instrumental Error of Automated Astronomical System on Landmark Azimuth Accuracy[1]

S. M. Tarasov*
Concern CSRI Elektropribor, JSC, St. Petersburg, Russia
**e-mail: sergione@list.ru*

Received January 13, 2021; revised April 8, 2021; accepted April 8, 2021

Abstract—The paper analyzes how random and systematic components of instrumental error of an automated astronomical system affect the accuracy of the landmark astronomical azimuth. The obtained results can be applied to construct the error mathematical model and to define the mutual orientation of the body axes when designing the system.

Keywords: astronomical azimuth, astronomical theodolite, instrumental error, simulation
DOI: 10.1134/S2075108721020085

INTRODUCTION

The attitude of objects in the geographical frame is commonly determined or monitored by gyroscopic aids measuring the astronomical azimuth such as gyrocompasses and gyrotheodolites [1–5]. They are periodically calibrated to reduce the systematic components of azimuth error [6, 7]. Calibration is done using a stationary astronomical azimuth determination system, which fastly and accurately determines the astronomical azimuth of reference direction by stellar observations [8–9]. However, its capabilities are limited by the operating conditions: it needs a specially equipped building on a massive vibroisolated foundation.

In field conditions, gyroscopic devices are calibrated using the reference directions specified by the landmarks (autocollimating reflectors or sighting targets) [2]. The azimuth of reference directions is determined by classical instruments: DKM-3A astronomical theodolite by Wild, Switzerland, and AU-1 automated astronomical system by the Central Research Institute of Geodesy, Airborne Survey and Cartography, Russia [2, 3, 10]. Azimuth determination is not automated in these devices, it requires long observations and highly qualified personnel.

High-precision total stations with stellar observation functions are also used in astrogeodetic surveys [11–13].

Satellite geodesy is also utilized in field determination of astronomical azimuth of reference direction. However, this method requires additional high-precision geodetic data (components of the deflection of the vertical). The accuracy of azimuth determination by this method depends on the distance between the observation points [14–16].

Currently, Concern CSRI Elektropribor develops an automated astronomical system (AAS) for precise and fast azimuth determination in field conditions. It is going to substitute the DKM-3A and AU-01 systems.

The AAS is designed as a classical astronomical theodolite comprising three main parts (Fig. 1):

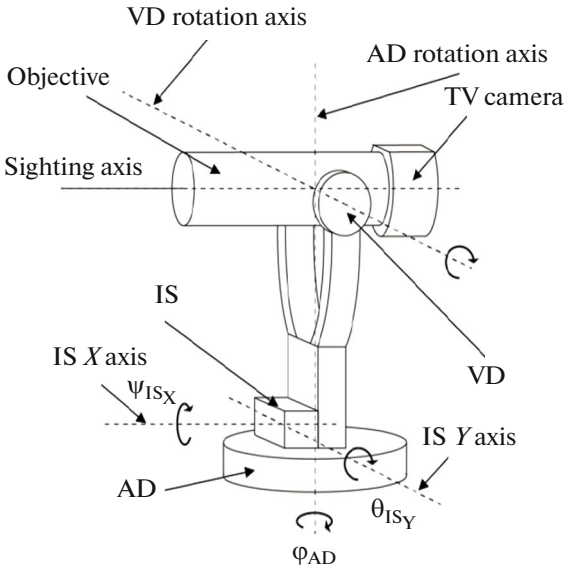

Fig. 1. AAS design and main components.

[1] The paper is based on presentation made at the 13th Multiconference on control Problems, Saint Petersburg, 2020.

• sighting device (SD) consisting of the objective and TV-camera;

• vertical drive (VD) rotating the sighting axis in the vertical plane;

• azimuth drive (AD) rotating the sighting axis in the horizontal plane.

The AAS also comprises a two-axis inclination sensor (IS) installed on the AD rotating part and a leveling system.

The AAS determines the landmark azimuth as follows: it determines the azimuth of sighting axis A_{SA} by stellar observations near the meridian plane and then turns it to the landmark, with the horizontal rotation angle of sighting axis γ calculated by AD angle sensor data. Thus the astronomical azimuth of a landmark is determined by the formula:

$$A_L = A_{SA} + \gamma. \quad (1)$$

Azimuth can be accurately determined only with proper mutual orientation of AD and VD rotation axes, IS sensitivity axes, and SD sighting axis. If the axes are improperly oriented due to technological errors in AAS manufacture and assembly, the horizontal error γ is determined with errors. Therefore, it is needed to analyze how AAS instrumental errors caused by technological defects in manufacture and assembly affect the azimuth determination accuracy.

LANDMARK AZIMUTH DETERMINATION ALGORITHM

The landmark azimuth determination algorithm can be conventionally divided into three major operations:

(a) determining the astronomical azimuth of the sighting axis during observation of near-meridian stars at the fixed altitude h_0;

(b) determining the horizontal angle γ when proceeding from the stellar observation to landmark observation;

(c) reversing the sighting axis: rotating it successively about AD rotation axis and then about VD rotation axis so that the sighting axis points the same side as before the rotations.

The sighting axis is reversed to reduce the systematic error components caused by IS bias and AAS technological errors in manufacture and assembly.

Operations a) and b) are performed before and after the reversal of the sighting axis to determine its azimuths A_{SA}^{I} and A_{SA}^{II}, and horizontal angles γ^{I} and γ^{II} (subscript "I" denotes prereversal position of the sighting axis, and "II", postreversal position).

The horizontal angle γ is calculated based on the changes in AD angle sensor data $\Delta\varphi_{AD}$ when proceeding from stellar to landmark observations.

The resultant astronomical azimuth of the landmark with account for the axis reversal is determined as

$$A_L = \frac{A_L^{I} + A_L^{II}}{2}, \quad (2)$$

where A_L^{I}, A_L^{II} are the landmark azimuth values before and after the reversal of the sighting axis, calculated by (1).

The astronomical azimuth of the sighting axis is determined as follows:

(1) the star images are recorded in the photodetector plane, and the arrays of coordinates of star image energy centers are generated $\{x_1, y_1 \ldots x_{N_{PD}}, y_{N_{PD}}\}$, where N_{PD} is the number of star images detected in the photodetector plane;

(2) initial equatorial coordinates α_0, δ_0 corresponding to the equatorial coordinates of the center of the working area in star catalogue are calculated using (3) for the stars north of zenith [10]

$$\alpha_0 = \theta_{GST} + \lambda_Z + 180^\circ; \ \delta_0 = 90^\circ - \varphi_Z + h_0, \quad (3)$$

and using (4) for the stars south of zenith

$$\alpha_0 = \theta_{GST} + \lambda_Z; \ \delta_0 = h_0 + \varphi_Z - 90^\circ, \quad (4)$$

where φ_Z, λ_Z are the astronomical coordinates of the location (initial data) that were earlier determined by the AAS by observing near-zenith stars similarly to the automated zenith telescope [17, 18], θ_{GST} is the Greenwich true siderial time [19, 20];

(3) the detected stars are identified by the coordinates of energy centers of their images in photodetector plane and star catalogue data, and the array of star pairs is generated, where the coordinates of star images $\{x_1, y_1 \ldots x_{N_{SP}}, y_{N_{SP}}\}$ in the photodetector plane are matched with their equatorial coordinates $\{\alpha_1, \delta_1 \ldots \alpha_{N_{SP}}, \delta_{N_{SP}}\}$ from the star catalogue and the calculated standard coordinates $\{\xi_1, \eta_1 \ldots \xi_{N_{SP}}, \eta_{N_{SP}}\}$, where N_{SP} is the number of identified stars [21]. Notably, the star equatorial coordinates from the star catalogue are determined with account for the star drift, astronomical refraction, parallax, aberration, and changes in the position of the celestial axis (precession and nutation) [19];

(4) parameters for transforming the coordinates from the photodetector plane to the standard coordinates (further, transformation parameters) are determined using the star pairs' array [22, 23];

(5) the coordinates of energy centers of star images with account for their declinations $\{\delta_1 \ldots \delta_{N_{SP}}\}$ are corrected for the shift during exposition caused by the Earth's daily rotation, and the transformation parameters are determined anew;

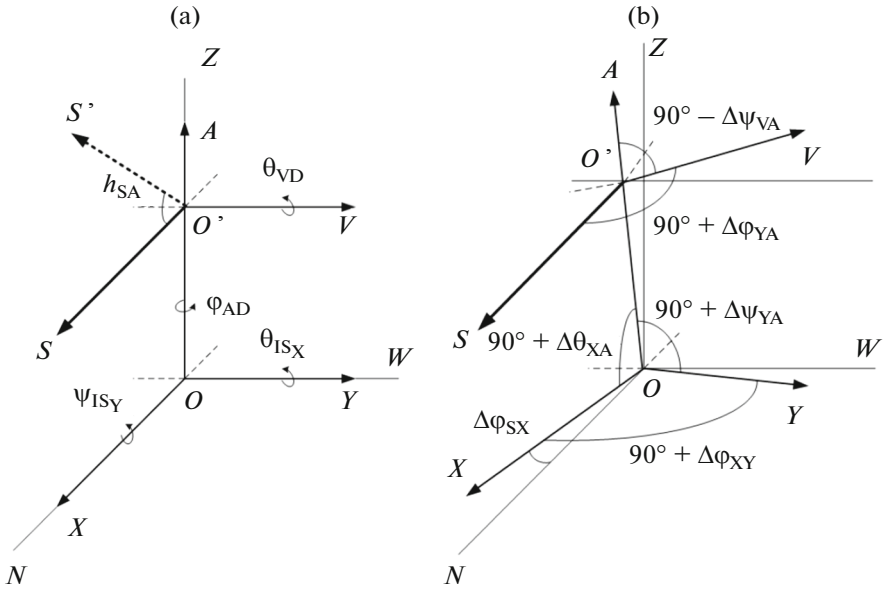

Fig. 2. AAS body axes in horizontal plane. (a) body axes in ideal position; (b) body axes under technological manufacturing errors.

(6) using the transformation parameters, the standard coordinates of the point on the celestial sphere corresponding to the photodetector center, and then its equatorial coordinates α_{SA}, δ_{SA} are determined [17];

(7) apparent azimuth A_{SA} and altitude h_{SA} of the sighting axis are determined using the following equations [20]:

$$A_{SA} = \arctan\left(\frac{\sin(s - \alpha_{SA})}{\sin(\varphi_Z)\cos(s - \alpha_{SA}) - \cos(\varphi_Z)\tan(\delta_{SA})}\right)$$
$$h_{SA} = \arccos\left(\frac{\cos(\delta_{SA})\sin(s - \alpha_{SA})}{\sin(A_{SA})}\right), \quad (5)$$

where $s = \theta_{GST} + 1.00274T - 0.00274\lambda_Z$ is the local sidereal time of the moment when the star images were recorded [24]; T is the local time, h.

(8) corrections to the astronomical azimuth for the tilt relative to the horizon plane ΔA_{tilt} in transverse direction (about the sighting axis) and for the shift x_P, y_P of the instantaneous pole with respect to the mean pole ΔA_{MP} are determined. Correction ΔA_{tilt} is calculated as

$$\Delta A_{tilt} = -\psi_{IS_Y}\tan(h_{SA}), \quad (6)$$

and correction ΔA_{MP} is determined as [1]

$$\Delta A_{MP} = -(x_P\sin\lambda_Z + y_P\cos\lambda_Z)\sec\varphi_Z; \quad (7)$$

(9) the resultant azimuth of the sighting axis using stellar observations is calculated as

$$A_{SA}^C = A_{SA} + \Delta A_{tilt} + \Delta A_{MP}. \quad (8)$$

COMPONENTS OF AAS INSTRUMENTAL ERROR

Mutual orientation of the AAS body axes and their position in the horizontal frame *ONWZ* is shown in Fig. 2. In the ideal case (Fig. 2a) with no technological manufacturing errors, the IS sensitivity axes (vectors *OX* and *OY*) lie within the horizon plane *NOW*. Vector *OA* coincides with the AD rotation axis, and vector *O'V,* with the VD rotation axis. Vector *O'S* corresponds to the position of the SD sighting axis when observing the landmark in the horizontal plane, then *O'S* is codirected with *OX*, and *O'V* is codirected with *OY*. Vector *O'S'* corresponds to the position of the sighting axis when observing the stars at the altitude h_{SA}, then orientation of the sighting axis in the horizontal frame *ONWZ* (astronomical azimuth A_{SA}, altitude h_{SA}) is determined by astronomical observations.

AD and VD angle sensors measure the rotation of the sighting axis *O'S* with respect to their zero positions (φ_{AD} and θ_{VD}, respectively). AAS tilt with respect

to the horizon plane is measured by IS in longitudinal and transverse directions (θ_{IS_X} and ψ_{IS_Y} respectively).

Figure 2b shows the position of the AAS body axes under technological manufacturing and assembly errors, where $\Delta\varphi_{SX}$ is the the horizontal angle between the projection of the sighting axis in the horizontal plane and IS *X* axis; $\Delta\varphi_{XY}$ is the horizontal angle characterizing the nonorthogonality of the IS axes; $\Delta\theta_{XA}$ is the vertical angle characterizing the nonorthogonality of IS *X* axis and AD rotation axis; $\Delta\psi_{YA}$ is the vertical angle characterizing the nonorthogonality of IS *Y* axis and AD rotation axis; $\Delta\varphi_{SV}$ is the horizontal angle characterizing the nonorthogonality of the sighting axis and VD rotation axis; $\Delta\psi_{VA}$ is the vertical angle characterizing the nonorthogonality of AD and VD rotation axes.

Along with technological manufacturing and assembly errors, the landmark azimuth error contains other components that can be expressed by RMS deviations for IS σ_{IS_X}, σ_{IS_Y}, VD angle sensor σ_{VD} and AD angle sensor σ_{AD}.

It is required to study how each of these error components influences the landmark azimuth accuracy.

SIGHTING AXIS ROTATIONS IN THE HORIZONTAL FRAME

In order to study how the instrumental error affects the accuracy of landmark astronomical azimuth, it is needed to mathematically describe the motion of the sighting axis in horizontal frame *ONWZ* when turning about AD and VD rotation axes.

Rotation about AD rotation axis by angle φ_{AD} in horizontal frame *ONWZ* is described by the following matrix [25]:

$$C_{\mu A}(\varphi_{AD}) = \begin{bmatrix} \cos(\varphi_{AD}) + B_A x_A^2 & B_A x_A y_A - \sin(\varphi_{AD}) z_A & B_A x_A z_A + \sin(\varphi_{AD}) y_A \\ B_A y_A x_A + \sin(\varphi_{AD}) z_A & \cos(\varphi_{AD}) + B_A y_A^2 & B_A y_A z_A - \sin(\varphi_{AD}) x_A \\ B_A z_A x_A - \sin(\varphi_{AD}) y_A & B_A z_A y_A + \sin(\varphi_{AD}) x_A & \cos(\varphi_{AD}) + B_A z_A^2 \end{bmatrix}, \quad (9)$$

where $B_A = 1 - \cos(\varphi_{AD})$; x_A, y_A, z_A are the Cartesian coordinates of vector *OA* (AD rotation axis) in *ONWZ* frame.

Coordinates x_A, y_A, z_A are calculated as follows:

$$\begin{bmatrix} x_A \\ y_A \\ z_A \end{bmatrix} = C^*_{\Delta\theta_{XA}} C^*_{\theta_{IS_X}} C^*_{\Delta\psi_{YA}} C^*_{\psi_{IS_Y}} \begin{bmatrix} x_{A0} \\ y_{A0} \\ z_{A0} \end{bmatrix}, \quad (10)$$

where $x_{A0} = 0$, $y_{A0} = 0$, $z_{A0} = 1$ are the coordinates of ideal vector *OA*; $C^*_{\theta_{IS_X}}$, $C^*_{\psi_{IS_Y}}$ are the rotation matrices for AAS tilt with respect to horizon plane θ_{IS_X}, ψ_{IS_Y}:

$$C^*_{\theta_{IS_X}} = C_{\theta_{IS_X}} C_{\Delta\varphi_{SX}}, \quad C^*_{\psi_{IS_Y}} = C_{\psi_{IS_Y}} C_{\Delta\varphi_{XY}}, \quad (11)$$

where

$$C_{\Delta\varphi_{SX}} = \begin{bmatrix} \cos(\Delta\varphi_{SX}) & -\sin(\Delta\varphi_{SX}) & 0 \\ \sin(\Delta\varphi_{SX}) & \cos(\Delta\varphi_{SX}) & 0 \\ 0 & 0 & 1 \end{bmatrix}, \quad C_{\Delta\varphi_{XY}} = \begin{bmatrix} \cos(\Delta\varphi_{XY}) & -\sin(\Delta\varphi_{XY}) & 0 \\ \sin(\Delta\varphi_{XY}) & \cos(\Delta\varphi_{XY}) & 0 \\ 0 & 0 & 1 \end{bmatrix}; \quad (12)$$

$$C_{\theta_{IS_X}} = \begin{bmatrix} \cos(\theta_{IS_X}) & 0 & -\sin(\theta_{IS_X}) \\ 0 & 1 & 0 \\ \sin(\theta_{IS_X}) & 0 & \cos(\theta_{IS_X}) \end{bmatrix}, \quad C_{\psi_{IS_Y}} = \begin{bmatrix} 1 & 0 & 0 \\ 0 & \cos(\psi_{IS_Y}) & -\sin(\psi_{IS_Y}) \\ 0 & \sin(\psi_{IS_Y}) & \cos(\psi_{IS_Y}) \end{bmatrix}; \quad (13)$$

$C^*_{\Delta\theta_{XA}}$, $C^*_{\Delta\psi_{YA}}$ are the rotation matrices for the angular deflections of the AAS body axes from their ideal positions, corresponding to technological errors $\Delta\theta_{XA}$, $\Delta\psi_{YA}$:

$$C^*_{\Delta\theta_{XA}} = C_{\Delta\theta_{XA}} C_{\Delta\varphi_{SX}}, \quad C^*_{\Delta\psi_{YA}} = C_{\Delta\psi_{YA}} C_{\Delta\varphi_{XY}}, \quad (14)$$

where

$$C_{\Delta\theta_{XA}} = \begin{bmatrix} \cos(\Delta\theta_{XA}) & 0 & -\sin(\Delta\theta_{XA}) \\ 0 & 1 & 0 \\ \sin(\Delta\theta_{XA}) & 0 & \cos(\Delta\theta_{XA}) \end{bmatrix}, \quad C_{\Delta\psi_{YA}} = \begin{bmatrix} 1 & 0 & 0 \\ 0 & \cos(\Delta\psi_{YA}) & -\sin(\Delta\psi_{YA}) \\ 0 & \sin(\Delta\psi_{YA}) & \cos(\Delta\psi_{YA}) \end{bmatrix}. \quad (15)$$

The similar matrix $C_{\mu V}(\theta_{VD})$ describes the rotation of vector $O'V$ – which has coordinates $x_{V0} = 0$, $y_{V0} = 1$, $z_{V0} = 0$ in the ideal position – about the VD rotation axis by angle θ_{VD}. Apart from the mentioned angles θ_{IS_X}, ψ_{IS_Y}, $\Delta\theta_{XA}$, $\Delta\psi_{YA}$, the orientation of VD rotation axis also depends on the rotation about AD rotation axis described by the matrix $C_{\mu A}(\varphi_{AD})$, and angles $\Delta\varphi_{SV}$, $\Delta\psi_{VA}$ described by the matrices

$$C_{\Delta\varphi_{SV}} = \begin{bmatrix} \cos(\Delta\varphi_{SV}) & -\sin(\Delta\varphi_{SV}) & 0 \\ \sin(\Delta\varphi_{SV}) & \cos(\Delta\varphi_{SV}) & 0 \\ 0 & 0 & 1 \end{bmatrix},$$
$$C_{\Delta\psi_{VA}} = \begin{bmatrix} 1 & 0 & 0 \\ 0 & \cos(\Delta\psi_{VA}) & -\sin(\Delta\psi_{VA}) \\ 0 & \sin(\Delta\psi_{VA}) & \cos(\Delta\psi_{VA}) \end{bmatrix}. \quad (16)$$

Then coordinates x_V, y_A, z_V are calculated as follows:

$$\begin{bmatrix} x_V \\ y_V \\ z_V \end{bmatrix} = C_{\mu A}(\varphi_{AD}) C_{\Delta\varphi_{SV}} C_{\Delta\psi_{VA}} C^*_{\Delta\theta_{XA}} C^*_{\theta_{IS_X}} C^*_{\Delta\psi_{YA}} C^*_{\psi_{IS_Y}} \begin{bmatrix} x_{V0} \\ y_{V0} \\ z_{V0} \end{bmatrix}. \quad (17)$$

Therefore, rotation of the sighting axis about AD rotation axis is described by the formula

$$\begin{bmatrix} x^R_{SA} \\ y^R_{SA} \\ z^R_{SA} \end{bmatrix} = C_{\mu A}(\varphi_{AD}) \begin{bmatrix} x_{SA} \\ y_{SA} \\ z_{SA} \end{bmatrix}, \quad (18)$$

and about VD rotation axis, by the formula

$$\begin{bmatrix} x^R_{SA} \\ y^R_{SA} \\ z^R_{SA} \end{bmatrix} = C_{\mu V}(\theta_{VD}) \begin{bmatrix} x_{SA} \\ y_{SA} \\ z_{SA} \end{bmatrix}, \quad (19)$$

where x_{SA}, y_{SA}, z_{SA} are the initial prerotation Cartesian coordinates of the sighting axis in horizontal frame; $x^R_{SA}, y^R_{SA}, z^R_{SA}$ are the postrotation Cartesian coordinates of the sighting axis in the horizontal frame.

SIMULATION

The systematic components of the instrumental error $\Delta\varphi_{SX}$, $\Delta\varphi_{XY}$, $\Delta\theta_{XA}$, $\Delta\psi_{YA}$, $\Delta\varphi_{SV}$, $\Delta\psi_{VA}$ were set within the range 60–360 arcsec. The random error components were simulated by processes with Gaussian distribution, zero mean values and RMS deviations σ_{IS_X} = 0.2 arcsec, σ_{IS_Y} = 0.2 arcsec, σ_{VD} = 60 arcsec, and σ_{AD} = 0.2 arcsec. The astronomical observations were simulated for the star sighting at $h_0 = 40°$, which is the optimal altitude. At higher altitude, the error in astronomical azimuth of the sighting axis grows, and at lower altitude, the effect of lateral refraction increases [10].

The simulation was performed as follows:

(1) the vectors corresponding to the body axes in ideal orientation (without instrumental errors) as shown in Fig. 2a were generated in the horizontal frame;

(2) instrumental errors $\Delta\varphi_{SX}$, $\Delta\varphi_{XY}$, $\Delta\theta_{XA}$, $\Delta\psi_{YA}$, $\Delta\varphi_{SV}$, $\Delta\psi_{VA}$ were set and the vectors corresponding to AD and VD rotation axes were generated using (9)–(17), then the tilt angles with respect to the horizon plane θ_{IS_X}, ψ_{IS_Y} were set as random processes with zero mean values and RMS deviations σ_{IS_X},σ_{IS_Y};

(3) using (19), the AAS sighting axis $O'S$ was turned to the position for observing the near-meridian stars by rotating the vector $O'S$ about VD rotation axis through the angle $\theta_{VD} = h_0 + \Delta\theta$, where $\Delta\theta$ is the error in VD rotation angle simulated as a random process with zero mean and RMS deviation σ_{VD}. After the sighting axis rotation about VD axis, its azimuth and altitude were calculated by the formulas

$$A_{SA} = \arcsin\left(\frac{y^R_{SA}}{\sqrt{(x^R_{SA})^2 + (y^R_{SA})^2}}\right);$$
$$h_{SA} = \arcsin\left(\frac{z^R_{SA}}{\sqrt{(x^R_{SA})^2 + (y^R_{SA})^2 + (z^R_{SA})^2}}\right), \quad (20)$$

(4) the readings of AD angle sensor φ_{AD} and the sighting axis azimuth during stellar observations A^I_{SA} were recorded, with AD angle sensor error simulated as a random process with zero mean and RMS deviation σ_{AD};

(5) true horizontal coordinates of the landmark (azimuth $A_L \in [0; 90]°$ and altitude $h_L = 0°$) were set and the sighting axis pointing at the landmark was simulated: the sighting axis was rotated about AD and VD axes so that its azimuth and altitude calculated by formulas (20) coincide with A_L and h_L. The axis was rotated about AD and VD axes using the formulas (18) and (19);

(6) after pointing at the landmark the data of AD angle sensor were calculated, and the horizontal rotation angle γ' was determined by the difference between the output during stellar observation and during the landmark observation. During the landmark observation, the error of AD angle sensor σ_{AD} was simulated;

(7) the landmark azimuth A^I_L was calculated using (1);

(8) reversal of the sighting axis was simulated: AAS body axes were successively rotated about AD rotation axis using the rotation matrix $C_{\mu A}$ by 180°, and then

Table 1. Systematic components of the instrumental error and their effects

$\Delta\varphi_{SX}$, arcsec	$\Delta\varphi_{XY}$, arcsec	$\Delta\theta_{XA}$, arcsec	$\Delta\psi_{YA}$, arcsec	$\Delta\varphi_{SV}$, arcsec	$\Delta\psi_{VA}$, arcsec	$\Delta_{A_L}^{syst}$, arcsec
60	60	60	60	60	60	**0.02**
120	120	120	120	120	120	**0.07**
180	180	180	180	180	180	**0.16**
240	240	240	240	240	240	**0.28**
300	300	300	300	300	300	**0.44**
360	360	360	360	360	360	**0.64**

Table 2. Random components of the instrumental error and their effects

σ_{IS_X}, arcsec	σ_{IS_Y}, arcsec	σAD, arcsec	σVD, arcsec	σ_{A_L}, arcsec
0	0	0	60	**0**
0.2	0	0	0	**0**
0	0.2	0	0	**0.12**
0.2	0.2	0	60	**0.12**
0	0	0.2	0	**0.20**
0.2	0.2	0.2	60	**0.23**

about the VD rotation axis using the matrix $C_{\mu V}$ by 180°;

(9) the sighting axis was again set to the meridian plane, the steps 3–7 were repeated, and the sighting axis azimuth during stellar observations A_{SA}^{II}, horizontal angle γ^{II} and azimuth of the landmark A_L^{II} after reversal were determined;

(10) the landmark azimuth A_L^{calc} was calculated using (2), then the azimuth error was estimated by the formula

$$\Delta A_L = A_L - A_L^{calc}. \quad (21)$$

As a result of simulation, the error array ΔA_L was formed comprising $N_K = 1000$ elements, and its mean value $\Delta_{A_L}^{syst}$ characterizing the systematic component of landmark azimuth error and RMS deviation σ_{A_L} characterizing the random error component were estimated.

SIMULATION RESULTS

The simulation was performed in Matlab environment.

Table 1 presents the simulated total effect of the technological manufacturing and assembly errors $\Delta\varphi_{SX}$, $\Delta\varphi_{XY}$, $\Delta\theta_{XA}$, $\Delta\psi_{YA}$, $\Delta\varphi_{SV}$, $\Delta\psi_{VA}$ on the systematic component of landmark azimuth error $\Delta_{A_L}^{syst}$. The maximum errors $\Delta_{A_L}^{syst}$ were observed for the case when the angular distance between the landmark and the meridian plane was $A_L = 90°$. The random components of the instrumental error were not specified.

The dependency of the landmark azimuth error on the angular distance between the landmark and the meridian plane is shown in Fig. 3.

Figure 4 presents the estimated effect produced by the individual components of the instrumental error and their combinations on the landmark azimuth accuracy as a percentage of the resultant $\Delta_{A_L}^{syst}$ depending on the angular distance between the landmark and the meridian plane.

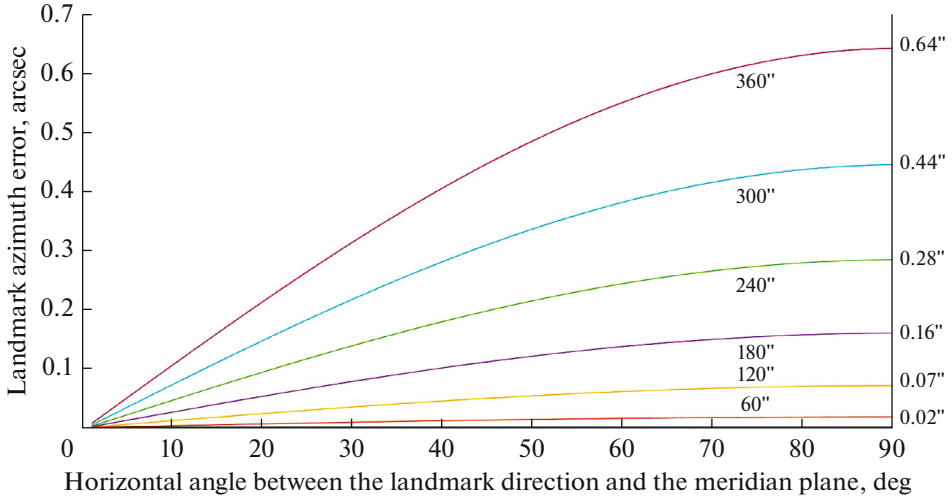

Fig. 3. Landmark azimuth error vs. angular distance between the landmark and the meridian plane.

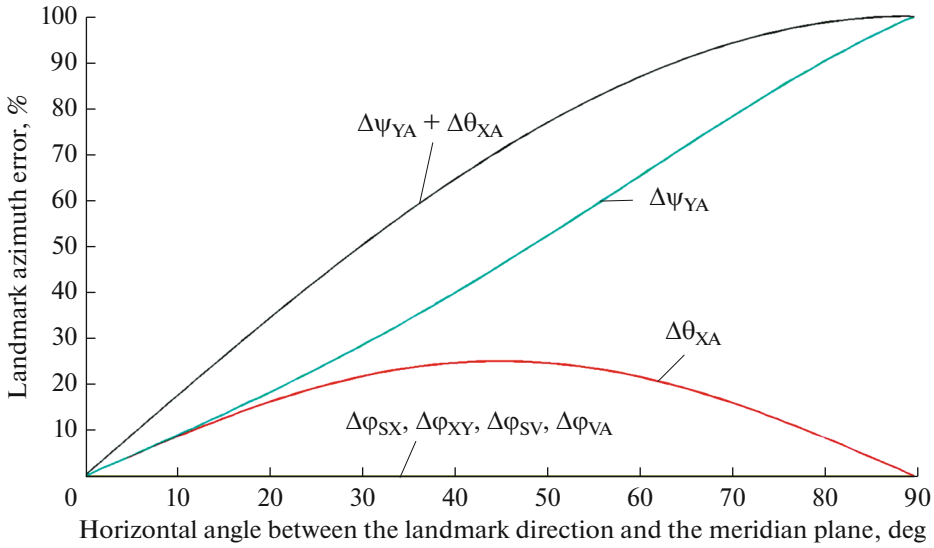

Fig. 4. Effect produced by the components of the instrumental error and their combinations as a percentage of the resultant error.

Table 2 presents the results of simulating the random components of the instrumental error: σ_{IS_X}, σ_{IS_Y}, σ_{VD} and σ_{AD}.

The following conclusions can be drawn from the simulation:

(1) the error systematic component $\Delta_{A_L}^{syst}$ depends on the angular distance between the landmark and the meridian plane and reaches maximum values when the angular distance is 90° (Fig. 3), with the astronomical observations conducted both north and south of zenith, when the azimuth $A_{SA} = 180°$;

(2) the main contribution to the error systematic component $\Delta_{A_L}^{syst}$ is made by the components of the instrumental error $\Delta\theta_{XA}$, $\Delta\psi_{YA}$ characterizing nonorthogonality of IS axes and AD rotation axis. The instrumental error components $\Delta\varphi_{SX}$, $\Delta\varphi_{XY}$, $\Delta\varphi_{SV}$, $\Delta\psi_{VA}$ produce a negligibly small effect (Fig. 4);

(3) IS error about axis X does not have a serious effect on the landmark azimuth error σ_{A_L}, and the effect of IS error about axis Y can be expressed as $\sigma_{IS_Y} \tan(h_{SA})\sqrt{2}/2$;

(4) the error of VD angle sensor σ_{VD} does not influence the landmark azimuth error σ_{A_L}, and AD angle sensor error σ_{AD} is completely included into σ_{A_L};

(5) the resultant random error component σ_{A_L} conditioned by the errors of AD and IS angle sensors can be expressed as

$$\sigma_{A_L} = \sqrt{\sigma_{AD}^2 + \frac{\sigma_{IS_Y}^2 \tan(h_{SA})^2}{2}}. \qquad (22)$$

CONCLUSIONS

The paper presents the results of simulating the effect produced by the instrumental error of the automated astronomical system on the accuracy of landmark azimuth determination. The results have demonstrated that the random component of azimuth error is mainly affected by the errors of the inclination sensor and angle sensor of the azimuth drive, and the systematic component is mostly affected by the vertical angles characterizing nonorthogonality of the inclination sensor axes and azimuth drive rotation axis. It is planned to further apply the obtained results to construct the mathematical model of the system error and form the requirements for mutual orientation of the system axes when designing the system.

ACKNOWLEDGMENTS

The author is grateful to N.V. Kuz'mina and V.V. Tsodokova for helpful remarks on the paper.

REFERENCES

1. *Rukovodstvo po astronomicheskim opredeleniyam* (A Guide on Astronomical Determinations), Moscow: Nedra, 1984.
2. *Rukovodstvo po astronomo-geodezicheskim rabotam pri topogeodezicheskom obespechenii voisk. Part 3. Giroskopicheskoe orientirovanie* (A Guide on Astronomical-Geodetic Surveys in Topographic-Geodetic Provision of Military Forces. Part 3. Gyroscopic Orientation), Moscow: RIO VTS, 1982.
3. Glazunov, A.S., *Modern tendencies in geodetic astronomy, Interexpo Geo-Siberia*, Novosibirsk: SGGA, 2008, pp. 183–188.
4. Bezdíček, V., Dandoš, R., Konečný, M., Kotrbanec, J., Král, T., and Wlochová, A., Orientation measurement

with gyrotheodolite, *Geodesy and Cartography*, 2018, vol. 44, p. 100–105.

5. Bezdíček, V., Dandoš, R., and Wlochová, A., Accuracy of determination of azimuth with a gyro-theodolite by the follow-up measurement, *Arabian Journal of Geosciences*, 2020, vol. 13.

6. Chernov, I.V., A procedure for determining the gyrotheodolite instrumental error with a preset accuracy, *Trudy voenno-kosmicheskoi akademii im. A.F. Mozhaiskogo* (Proceedings of the Mozhaiskiy Military Space Academy), St. Petersburg: Mozhaiskiy Military Space Academy, 2019, No. 671, pp. 192–200.

7. Chernov, I.V., Determining the orientation accuracies achieved by gyrotheodolite systems, *Naukoemkie tekhnologii v kosmicheskikh issledovaniyakh Zemli* (High Technologies in Space Surveys of the Earth), 2016, vol. 8, no. 6, pp. 12–16.

8. Gayvoronskii, S.V., Kuz'mina, N.V., and Tsodokova, V.V., A high-precision optoelectronic system for determining the astronomical azimuth: Development results, *Materialy dokladov 28 konferentsii pamyati N.N. Ostryakova* (Proceedings of the 28th Conference in Memory of N.N. Ostryakov), St. Petersburg: Concern CSRI Elektropribor, JSC, 2012.

9. Gayvoronskii, S.V., Berkovich, S.B., Kotov, N.I., Makhaev, A.Yu., Sadekov, R.N., and Tsodokova, V.V., An automatic system for determining astronomical azimuth, *Measurement Techniques*, 2015, vol. 58, no. 3, pp. 280–285.

10. Gienko, E.G., *Astrometriya i geodezicheskaya astronomiya* (Astrometry and Geodetic Astronomy), Novosibirsk: SGGA, 2011.

11. Hauk, M., Hirt, C., and Ackermann, C., Experiences with the QDaedalus system for astrogeodetic determination of deflections of the vertical, *Survey Review*, 2016, vol.49, pp. 294–301.

12. Baladimos, D.D., Korakitis, R., Lambrou, E., and Pantazis, G., Fast and accurate determination of astronomical coordinates Φ, Λ and azimuth using a total station and GPS receiver, *Survey Review*, 2003, vol. 37, pp. 269–275.

13. Lambrou, E. and Pantazis, G., Astronomical azimuth determination by the hour angle of Polaris using ordinary total stations, *Survey Review,* vol. 40, 2008, p. 164–172.

14. Chernov, I.V., The model of integrated satellite-gyroscopic system for fast determination of astronomical azimuth, *Geodeziya i kartografiya* (*Geodesy and Cartography*), 2017, vol. 78, no. 7, pp. 2–8.

15. Sholokhov, A.V., Berkovich, S.B., Kotov, N.I., and Makhaev, A.Yu., Determining the achievable azimuth determination accuracy with a short baseline using satellite and geodetic aids, *Geodeziya i kartografiya* (*Geodesy and Cartography*), 2018, vol. 79, no. 6, pp. 2–8.

16. Chang, C.C. and Tsai, W.Y., Evaluation of a GPS-based approach for rapid and precise determination of geodetic/astronomical azimuth, *Journal of Surveying Engineering*, 2016.

17. Tsodokova, V. V., Gaivoronskii, S.V., Tarasov, S.M., and Rusin, E.V., Determination of astronomical coordinates with an automated zenith telescope, *16 Konferentsiya molodykh uchenykh "Navigatsiya i upravlenie dvizheniem"* (Proceedings of the 16th Conference of Young Scientists "Navigation and Motion Control"), St. Petersburg: Concern CSRI Elektropribor, JSC, 2014, pp. 269–276.

18. *Modern Technologies and Methods for Measuring the Earth's Gravity Field Parameters*, Peshekhonov, V.G., Stepanov, O.A., Eds., St. Petersburg: Concern CSRI Elektropribor, JSC, in press.

19. Brumberg, V.A., Glebova, N.I., Lukashova, M.V., Malkov, A.A., Pit'eva, E.V., Rumyantseva, L.I., Sveshnikov, M.L., and Fursenko, M.A., *Trudy IPA RAN. Vypusk 10.* (Proceedings of IAA RAS. No. 10. Detailed Explanation of the Astronomical Yearbook), St. Petersburg: IAA RAS, 2004.

20. Kovalevskii, Zh., *Sovremennaya astrometriya* (Modern Astrometry), Fryazino: Vek 2, 2004.

21. Gaivoronskii, S.V., Rusin, E.V., and Tsodokova, V.V., Comparative analysis of algorithms for star identification in an image, *16 Konferentsiya molodykh uchenykh "Navigatsiya i upravlenie dvizheniem"* (Proceedings of the 16th Conference of Young Scientists "Navigation and Motion Control"), St. Petersburg: Concern CSRI Elektropribor, JSC, 2014, pp. 284–290.

22. Tsodokova, V.V. and Motorin, A.V., Calculation of accuracy characteristic in estimation of parameters of the star coordinates transformation, *Izvestiya Tul'skogo gosudarstvennogo universiteta* (Proceedings of Tula State University), 2016, pp. 129–141.

23. Tsodokova, V.V. and Motorin, A.V., Analysis of accuracy of determining the parameters of the star coordinates transformation, *18 Konferentsiya molodykh uchenykh "Navigatsiya i upravlenie dvizheniem"* (Proceedings of the 18th Conference of Young Scientists "Navigation and Motion Control"), St. Petersburg: Concern CSRI Elektropribor, JSC, 2016, pp. 416–424.

24. Blazhko, S.N. *Kurs prakticheskoi astronomii* (A Course of Practical Astronomy), Moscow: Nauka, 1979, pp. 393–408.

25. Matveev, V.V. and Raspopov, V.Ya., *Osnovy postroeniya besplatformennykh inertsial'nykh navigatsionnykh sistem* (Fundamentals of Designing Strapdown Inertial Navigation Systems), Raspopov, V.Ya., Ed., Concern CSRI Elektropribor, JSC, St. Petersburg, 2009.